BIOCHEMISTRY
including biophysical chemistry & molecular biology

Article

pubs.acs.org/biochemistry

Anion-Dependent Stimulation of CYP3A4 Monooxygenase

Irina F. Sevrioukova*,† and Thomas L. Poulos†,‡,§

Departments of †Molecular Biology and Biochemistry, ‡Chemistry, and §Pharmaceutical Sciences, University of California, Irvine, California 92697-3900, United States

Supporting Information

ABSTRACT: We co-crystallized human cytochrome P450 3A4 (CYP3A4) with progesterone (PRG) under two different conditions, but the resulting complexes contained only one PRG molecule bound to the previously identified peripheral site. A novel feature in one of our structures is a citrate ion, originating from the crystallization solution. The citrate-binding site is located in an area where the N-terminus splits from the protein core and, thus, is suitable for the interaction with the anionic phospholipids of the microsomal membrane. We investigated how citrate affects the function of a soluble CYP3A4 monooxygenase system consisting of equimolar amounts of CYP3A4 and cytochrome P450 reductase (CPR). Citrate was found to affect the properties of both redox partners and stimulated their catalytic activities in a concentration-dependent manner via a complex mechanism. CYP3A4−substrate binding, reduction of CPR with NADPH, and interflavin and interprotein electron transfer were identified as citrate-sensitive steps. Comparative analysis of various negatively charged organic compounds indicated that, in addition to alterations caused by changes in ionic strength, anions modulate the properties of CYP3A4 and CPR through specific anion−protein interactions. Our results help to better understand previous observations and provide new mechanistic insights into CYP3A4 function.

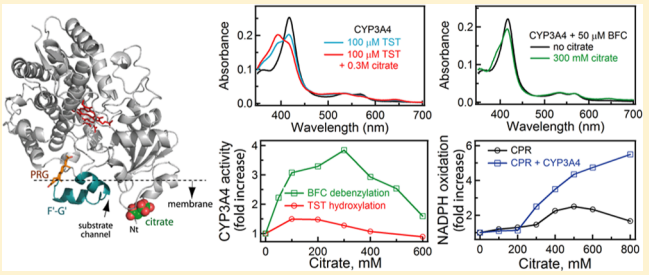

Human cytochrome P450 3A4 (CYP3A4) is the major xenobiotic-metabolizing enzyme implicated in oxidation and clearance of a vast variety of drugs and other foreign compounds.[1,2] Like most mammalian P450s, CYP3A4 is anchored to the lipid bilayer via the N-terminal transmembrane fragment. An additional hydrophobic surface through which CYP3A4 interacts with the membrane is thought to be the F′-G′ helix/loop region located near the opening of the substrate access channel. Such spatial organization could assist translocation of hydrophobic substrates from the membrane into the CYP3A4 active site, which is capable of accommodating a wide range of molecules varying in size and chemical structure.

It has been proposed that atypical kinetic behavior and allosterism of CYP3A4, manifested as nonlinear or sigmoidal substrate-binding titration plots or the reaction rate vs substrate concentration dependence,[1,3−5] are caused by simultaneous binding of two or more molecules of the same or different nature. The available X-ray data indicate that two inhibitor molecules can simultaneously bind to the CYP3A4 active site cavity.[6,7] Crystallization of functional complexes with substrates is more challenging because most of the known CYP3A4 substrates have low affinity and poor aqueous solubility and, as we have found, tend to dissociate from the active site during crystallization. Currently, only the erythromycin-, bromoergocryptine-, and progesterone (PRG)-bound structures of CYP3A4 have been determined,[6,8,9] but only bromoergocryptine associates in a productive mode. Erythromycin binds within the active site cavity, but its site of metabolism is 17 Å away from the heme.[6] PRG, on the other hand, docks to a hydrophobic surface cleft, predicted to be embedded into the membrane.[10,11] Based on the crystal structure, the PRG-binding site was proposed to be functionally important and serve as a substrate/effector recognition area,[8] which agrees with the experimental data showing that replacement of Leu211 and Asp214, located in the vicinity of PRG in the crystal structure, with bulkier residues affects cooperativity in the PRG binding and metabolism.[12]

We co-crystallized CYP3A4 with PRG under two different conditions, but in both complexes, there was only one PRG molecule docked at the previously identified peripheral site.[8] Here, we provide a more detailed analysis of the PRG-binding area and describe a novel citrate-binding site. To test if/how citrate and other natural anionic compounds affect the function of CYP3A4, we analyzed the metabolism of 7-benzyloxy-4-(trifluoromethyl)coumarin (BFC) and testosterone (TST) in a lipid-free reconstituted system with cytochrome P450 reductase (CPR), as well as individual properties of the redox partners. Here, we report that anions modulate the activity of both CYP3A4 and CPR, and discuss the physiological relevance of these findings.

EXPERIMENTAL PROCEDURES

Protein Expression and Purification. The C-terminally 4-histidine tagged wild-type (WT), Δ3−22, and Δ3−28 human

Received: May 8, 2015
Revised: June 9, 2015
Published: June 11, 2015

DOI: 10.1021/acs.biochem.5b00510
Biochemistry 2015, 54, 4083−4096

CYP3A4 were produced, purified, and quantified as reported elsewhere.[13] CPR and its Δ1−74 catalytic domain (trCPR) were purified according to previously reported procedures.[14,15]

CYP3A4 Crystallization. Δ3−22 CYP3A4 was co-crystallized with PRG at room temperature by a hanging drop vapor diffusion method. CYP3A4 (65 mg/mL) in 100 mM phosphate, pH 7.4, 20% glycerol and 100 mM NaCl was incubated with a 4-fold excess of PRG (dissolved in dimethyl sulfoxide) and centrifuged to remove the precipitate. A crystallization drop consisted of 0.5 μL of the protein solution and 0.5 μL of either the mixture containing 6% PEG 3350, 20 mM Bis-Tris propane, pH 6.4, 12 mM ammonium citrate, and 5% glycerol or solution no. 11 from the Hampton Research PegIon2 kit containing 12% PEG 3350 and 4% Tacsimate, pH 5.0. Crystals were harvested 2 to 3 days after setup and cryoprotected with Paratone-N before freezing in liquid nitrogen. X-ray diffraction data were collected at the Stanford Synchrotron Radiation Lightsource, beamline 11-1, and the Advanced Light Source, beamline 8.2.2. Structures were solved by molecular replacement with PHASER[16] and 1TQN as a search model. The initial models were refined with COOT[17] and PHENIX.[18] Data collection and refinement statistics are summarized in Supporting Information Table S1. The atomic coordinates and structure factors for the CYP3A4−PRG and CYP3A4−PRG−citrate complexes were deposited to the Protein Data Bank with ID codes 5A1R and 5A1P, respectively.

Spectral Measurements. Substrate-induced spectral changes in CYP3A4 were monitored on a Cary 300 spectrophotometer in 100 mM phosphate, pH 7.4, in the absence or presence of various anionic compounds. TST, BFC, and sodium salts of all organic acids utilized in this study were purchased from Sigma-Aldrich. Anion solutions were buffered to pH 7.4 before use. During equilibrium titrations, small aliquots of dimethyl sulfoxide solutions of TST (final solvent concentration <2%) were added to CYP3A4 in the presence and absence of 300 mM citrate. Titration plots were analyzed using the Hill equation to derive the Hill coefficient (n_H) and the TST concentration producing half occupation (S_{50}).

TST Binding Kinetics. The rate of TST binding to CYP3A4 was measured in a SX.18MV stopped-flow apparatus (Applied Photophysics) by following a low-to-high spin transition in the heme iron. A solution of 2 μM CYP3A4 in 100 mM phosphate, pH 7.4, with or without 300 mM citrate was mixed with 5−200 μM TST, and an absorbance decrease at 418 nm was monitored over time. Kinetic data were analyzed using the IgorPro program (WaveMetrics, Inc.).

CYP3A4 Activity Assays. The BFC O-debenzylase activity of CYP3A4 was assessed fluorimetrically in a lipid-free reconstituted system with CPR. The reaction was carried out at room temperature in 100 mM phosphate, pH 7.4, containing catalase and superoxide dismutase (2 units/mL each) in the absence or presence of anions. A mixture of CYP3A4 and CPR (1 μM each) was preincubated at room temperature and diluted 20-fold with the assay buffer before measurements. BFC (50 μM final concentration) was added 2 min prior initiation of the reaction with 100 μM NADPH. Formation of 7-hydroxy-4-(trifluoromethyl) coumarin (HFC; λ_{ex} = 404 nm; λ_{em} = 500 nm) was monitored for 2 min using a Hitachi F100 fluorimeter. The reaction rates were estimated based on the HFC calibration curve (0.02−0.5 μM) obtained under identical experimental conditions.

Turnover for the CYP3A4-dependent TST hydroxylation was measured by liquid chromatography coupled to mass spectrometry[19] with some modifications. The incubation solution (1 mL) contained 100 mM phosphate buffer, pH 7.4, catalase and superoxide dismutase (2 units/mL each), 100 μM TST, 1 μM CYP3A4, 1 μM CPR, various concentrations of citrate, and the NADPH-generating system consisting of 10 mM glucose, 0.2 mM $NADP^+$, and glucose-6-phosphate dehydrogenase (2 units/mL; Sigma-Aldrich). The reaction was carried out for 10 min at 37 °C and quenched with 2.5 mL of dichloromethane. After addition of 1 mL of 0.3 M NaCl, samples were vigorously mixed and centrifuged for 10 min at 3000*g* at room temperature. The bottom organic phase (2 mL) was transferred to a clean vial, evaporated under a nitrogen stream, and dissolved in 140 μL of 50% acetonitrile. Samples were analyzed on a Waters Acquity UPLC C_{18} BEH column (2.1 × 50 mM, 1.7-particle size) attached to the Waters Acquity Ultra Performance LC System. The UPLC was in line with a tandem quadrupole mass spectrometer (Waters Micromass Premier XE; Waters, USA) operated in positive ion mode. Peaks were separated with a linear gradient of mobile phases A (98% water, 2% acetonitrile, 0.2% acetic acid, and 5 mM ammonium acetate) and B (100% acetonitrile, 0.2% acetic acid, and 5 mM ammonium acetate) at 0.3 mL/min. The gradient started at 90% A (0.5 min), after which solvent B was linearly increased from 10 to 95% (0.5−3 min). The cone and collision energies were 25 V and 15 eV, respectively. The precursor to fragment ions was singly positively charged hydroxy-TST (305 m/z). TST metabolites produced in the reconstituted system were identified using commercially available hydroxy-TST standards obtained from Steraloids (USA). Three major peaks on the chromatograms with elution times of 1.08, 1.15, and 1.35 min corresponded to 6β-hydroxy-TST, 16β-hydroxy-TST, and TST, respectively. Concentrations of 6β-hydroxy-TST and 16β-hydroxy-TST produced by CYP3A4 were estimated based on fragment ions with m/z of 173 and 109, respectively.

Kinetics of CYP3A4 Reduction with CPR. Kinetics of CYP3A4 reduction with CPR was measured at ambient temperatures on a Cary 300 spectrophotometer using an anaerobic cuvette with a stirring bar. All solutions contained 50 mM phosphate, pH 7.4, and an oxygen scavenging system consisting of 10 mM glucose, glucose oxidase, and catalase (5 units/mL each). After degassing, the reaction mixture in a sealed cuvette was saturated with CO. Reduction of 1 μM CYP3A4 with 1 μM CPR was followed at 448 nm to monitor formation of the Fe^{2+}-CO adduct upon injection of NADPH (100 μM final concentration). Kinetic data were analyzed with SigmaPlot.

Kinetics of CPR Reduction with NADPH. NADPH-dependent spectral changes in CPR were measured at 3 °C on a SX.18MV stopped-flow apparatus (Applied Photophysics). Kinetic data were collected as a function of logarithmic time using a single wavelength or diode array detection mode. All experiments were carried out under anaerobic conditions in the presence of an oxygen scavenging system described above. CPR (15 μM) was mixed with a 10-fold excess of NADPH in 50 mM phosphate buffer, pH 7.4, in the absence or presence of 100−600 mM citrate. Single-wavelength kinetics were recorded at 456, 600, and 730 nm to follow flavin reduction and formation of the flavin semiquinone species and $NADP^+$−$FADH^-$ charge-transfer complex, respectively. Diode array spectra were recorded using an integration time of 2.56 ms. Data were analyzed with Pro-K software (Applied Photophysics).

DOI: 10.1021/acs.biochem.5b00510
Biochemistry 2015, 54, 4083−4096

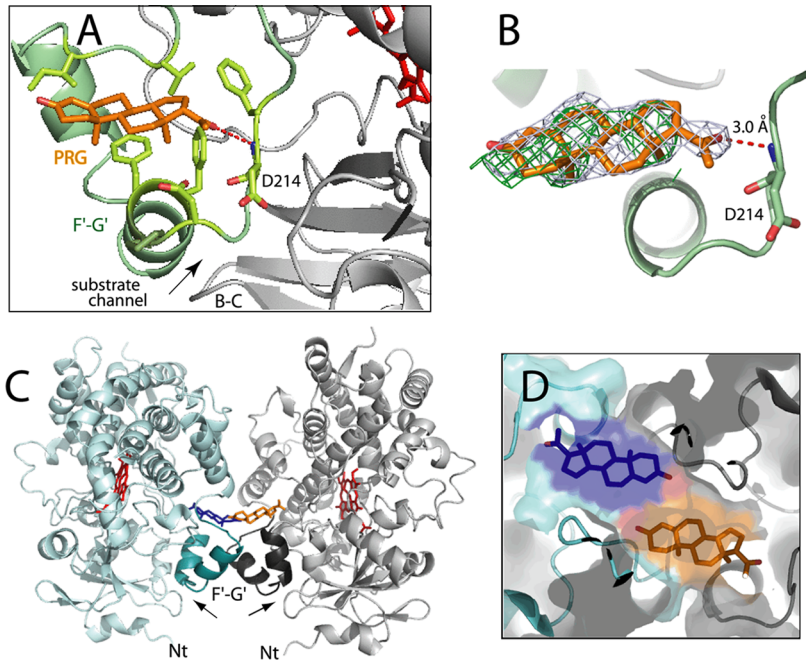

Figure 1. Crystal structure of the CYP3A4–PRG complex determined at 2.45 Å resolution. This structure is virtually identical to the 1W0F model, with an rmsd of 0.53 Å between C_α atoms. (A) Peripheral PRG-binding site. The F′-G′-helix/loop region is in green, heme is in red, and PRG is in orange. A hydrogen bond between the acetyl oxygen of PRG and the amide nitrogen of Asp214 is shown as a red dotted line. (B) Close-up view at PRG with the $2F_o - F_c$ and omit maps contoured at the 1σ and 3σ levels (in blue-gray and green, respectively). (C) Crystallographic dimer formed between CYP3A4 and the symmetry-related molecule. Arrows show the entrance into the substrate-binding channel. (D) Different and magnified view of the PRG-binding site. PRG binds at the crystallographic interface and makes contacts with the symmetry-related CYP3A4 and PRG molecules. The majority of the intermolecular contacts are mediated by nonpolar residues from the F′-G′-peptides, highlighted in brighter shades of cyan and gray.

CPR Activity and Fluorescence Assays. The effect of citrate and other natural anionic compounds on the CPR-dependent NADPH oxidation was determined spectrophotometrically at ambient temperatures. Absorbance changes were monitored at 340 nm (ε = 6.22 μM^{-1} cm^{-1}) after addition of 1 mM NADPH to the solutions of 2 μM CPR in the absence or presence of various concentrations of anions and 2 μM WT or trCYP3A4. Electron transfer to cytochrome *c* was followed at 550 nm (ε = 21 μM^{-1} cm^{-1}). Anion-dependent changes in the fluorescence yield of 5 μM CPR or free FMN were measured on a Hitachi F100 fluorimeter (λ_{ex} = 450 nm; λ_{em} = 520 nm) in the presence and absence of 300 mM anions and equimolar amounts of CYP3A4. All experiments on CPR were conducted in 50 mM phosphate, pH 7.4.

Gel Filtration. Gel filtration experiments were conducted at 4 °C in 100 mM phosphate, pH 7.4, in the absence and presence of 300 mM citrate using an FPLC Superdex 200 column (0.9 × 30 cm; GE Healthcare) with a 0.3 mL/min flow rate. Elution of WT and trCYP3A4, CPR or a 1:1 CPR–CYP3A4 mixture (15 nmole each) was monitored at 417 or/and 452 nm to follow the heme and flavin absorption, respectively. Oxidized and NADH-reduced apoptosis inducing factor (62 and 125 kDa, respectively), nitric oxide synthase (320 kDa), and ferritin (440 kDa) were used as molecular standards.

RESULTS

Progesterone Binding Site Is Located at the Crystallographic Interface. A peripheral PRG-binding site was first identified in the crystal structure reported by Williams and coworkers (PDB ID 1W0F).[8] We co-crystallized CYP3A4 with PRG under two different conditions, but in the same *I*222 space group, with one protein molecule per asymmetric unit. Similar to the 1W0F model, both of our structures contain only one PRG molecule docked at the same peripheral site above the Phe-cluster and H-bonded to the amide nitrogen of Asp214 (Figure 1A, B). Importantly, PRG binds at the interface between symmetry-related CYP3A4 molecules (Figure 1C,D). The intermolecular surface is predominantly hydrophobic and formed by residues from the outer surface of the F′-G′ helices and a symmetry-related PRG. Without these symmetry contacts, a large portion of PRG would be exposed and, hence, its binding affinity should be weaker in the CYP3A4 monomer. This important feature of the CYP3A4–PRG crystal structure was omitted in the original publication,[8] where the PRG docking area was proposed to be functionally important and serve as an effector binding site.

Citrate Binding Site. A novel feature observed in one of our CYP3A4–PRG structures (PDB ID 5A1P) is a citrate-binding site (Figure 2A,B). Citrate originates from the crystallization buffer and attaches to the area where the N-terminal peptide separates from the protein core. The complex is stabilized through five hydrogen bonds formed between the carboxylate oxygens of citrate and the side and main chain atoms of Ser29, His30, Phe46, and Gln78 (Figure 2C). Owing to these specific interactions at a strategic location, the citrate-binding area is suitable for association with the head groups of negatively charged phospholipids, critical for the CYP3A4 incorporation into the lipid bilayer, activity, and CYP3A4–CPR interaction.[20−22] It also is known that CYP3A4 can be activated in the presence of high phosphate concentrations.[23] Since citrate is a natural anion abundantly present in the cell, we

DOI: 10.1021/acs.biochem.5b00510
Biochemistry 2015, 54, 4083−4096

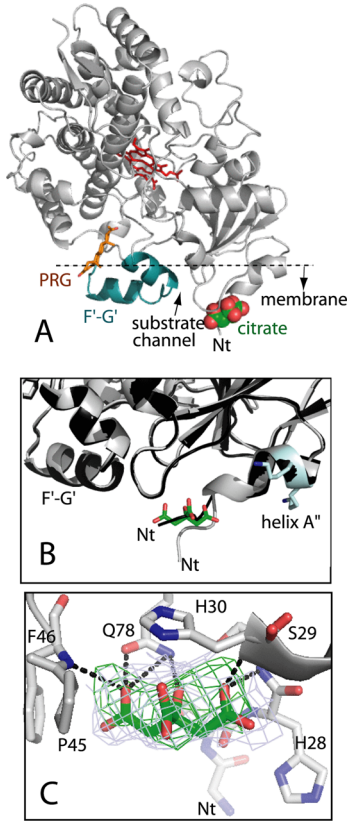

Figure 2. Citrate-binding site observed in one of the newly determined CYP3A4–PRG structures solved at 2.5 Å resolution. (A) Citrate originates from the crystallization solution and binds between the protein core and the N-terminal tail. A dashed line shows the predicted level of CYP3A4 incorporation into the membrane.[11] Such membrane topology is inconsistent with the crystallographic dimer of CYP3A4 depicted in Figure 1C. (B) Superposition of the citrate-free and citrate-bound CYP3A4–PRG complexes (in black and light gray, respectively) showing how citrate (in green) changes orientation of the N-terminal peptide. Lys34 and Lys35 from the A″-helix (in cyan) as well as the citrate-binding area could mediate interaction with the negatively charged phospholipids, known to be critical for the membrane incorporation and activity of CYP3A4.[20−22] (C) Hydrogen-bonding interactions formed between citrate and surrounding residues. The $2F_o - F_c$ and omit electron density maps contoured around citrate at 1σ and 3σ are displayed in blue-gray and green, respectively.

tested whether it has any effect on CYP3A4 catalysis. In all experiments described below, 50 or 100 mM phosphate was used as an initial assay buffer (specified in the Experimental Procedures), to which various amounts of buffered anion solutions were added to reach the desired concentration.

Citrate Stimulates Catalytic Activity of CYP3A4. To catalyze chemical reactions, CYP3A4 and other microsomal P450s require CPR as an electron donor (Figure 3) and, in some cases, cytochrome b_5. The monooxygenase activity of CYP3A4 can be fully reconstituted in proteoliposomes and partially in lipid-free solutions. For easier data interpretation, we used a simplified reconstituted system consisting of equimolar amounts of soluble CYP3A4 and CPR. The effect of citrate on BFC and TST metabolism was assessed for the full-length (WT) and membrane linker-free Δ3–28 CYP3A4 (trCYP3A4). The citrate-binding site is preserved in both protein forms and, therefore, dissimilarities in their catalytic and molecular properties can be attributed to the presence/absence

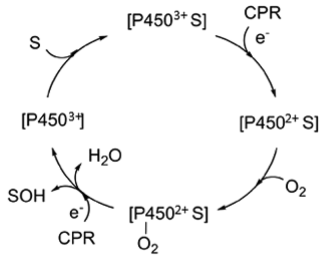

Figure 3. Catalytic cycle of cytochrome P450. P450^{3+}, resting state; S, substrate; [P450^{3+}–S], substrate-bound ferric form; [P450^{2+}–S], substrate-bound ferrous form; [O_2–P450^{2+}–S], dioxygen- and substrate-bound ferrous form; SOH, hydroxylated substrate. In mammalian P450 monooxygenase systems, electrons are delivered by CPR.

of the N-terminal peptide. Citrate was found to stimulate BFC debenzylation catalyzed by both the full-length and truncated CYP3A4, although to a different extent (Figure 4A,B). The turnover number for WT CYP3A4 reached the maximum of 0.02 min^{-1} at 300 mM citrate and then declined, whereas the trCYP3A4 activity was 2-fold lower at the start but gradually increased within the entire concentration range and reached that of WT. As a result, the activation degree for trCYP3A4 was markedly higher: 34- vs 4-fold for WT at 600 mM citrate (Figure 4B).

A similar trend was observed for TST metabolism (Figure 4C,D), which, overall, was over 100-fold more effective but influenced by citrate to a lesser extent than the BFC debenzylation reaction, with 1.5- and 3-fold activation of WT and trCYP3A4, respectively. Again, the intermediate citrate concentrations (100–200 mM) were optimal for WT, whereas the trCYP3A4 activity was maximal at 400–600 mM citrate. The product profile, however, did not depend on the protein length or citrate concentration, as 6β- and 16β-hydroxy-TST were found to be the main metabolites under all conditions tested (~95 and 5% of the total product, respectively). Considering the higher anion sensitivity of trCYP3A4 and the fact that citrate activates CYP3A4 at concentrations 4 orders of magnitude higher than that needed for saturation of the crystallographic citrate-binding site (citrate/CYP3A4 ratio of (3–6) × 10^5:1 and 20:1, respectively), we conclude that citrate stimulates soluble CYP3A4 via a mechanism that does not involve the membrane linker or the citrate-binding area observed in the crystal structure.

Effect of Other Anionic Compounds on BFC Metabolism. To identify other potential activators of CYP3A4, we screened a series of natural anionic compounds that included glycerol 3-phosphate (or glycerophosphate), acetate, formate, succinate, malate, and phosphate, a known stimulator of the CYP3A4 activity,[23] as well as NaCl as a control. It was found that all anions except acetate promote BFC metabolism, with the highest turnover observed at ~300 mM concentrations (Figure 5). Glycerophosphate and malate had the most pronounced activatory effect, which was close to that of citrate. That NaCl stimulates CYP3A4 nearly as well as citrate and other compounds implies that anions exert their action, in part, by altering ionic strength, which is proportional to the ion concentration (c) and its charge (z): $I = {}^1/_2 cz^2$.

In 300 mM solutions of singly, doubly, and triply charged molecules, the I values will be 300, 600, and 900 mM, respectively, and isocratic solutions of the phosphate group containing compounds or mono- or dicarboxylic acids should

DOI: 10.1021/acs.biochem.5b00510
Biochemistry 2015, 54, 4083–4096

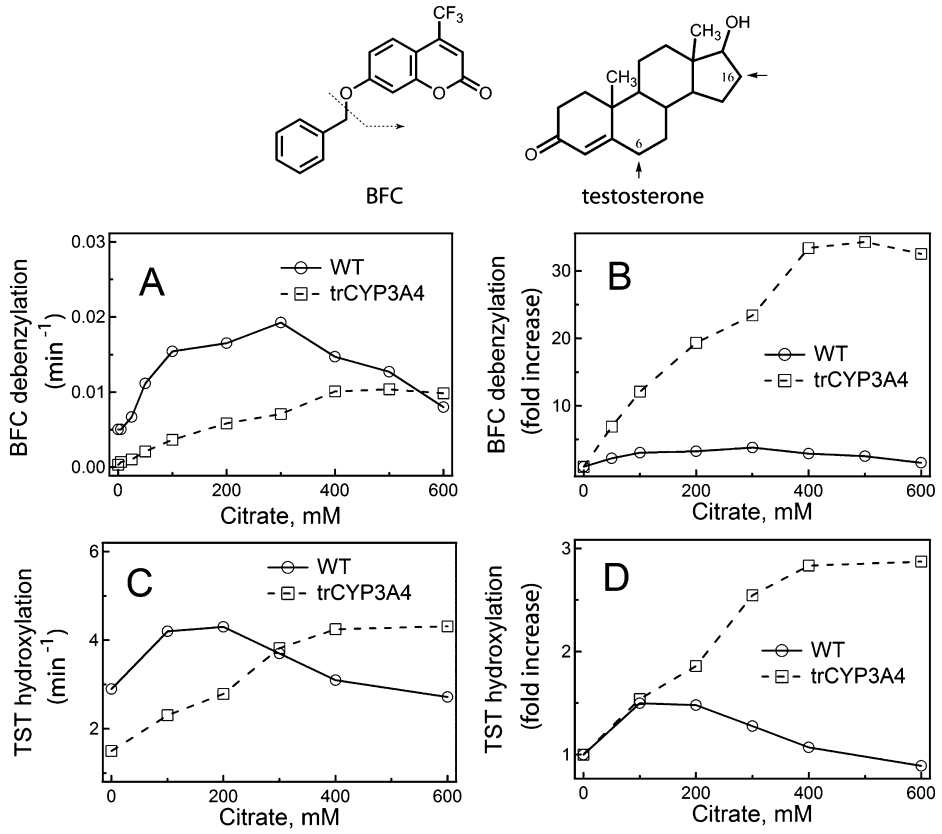

Figure 4. Effect of citrate on the BFC debenzylation and TST hydroxylation reactions catalyzed by WT and trCYP3A4. Assay conditions are described in the Experimental Procedures. Arrows indicate the sites of metabolism in BFC and TST. 6β-Hydroxy-TST is the major product of TST metabolism (~95% of the total product). Citrate stimulates the catalysis of both WT and trCYP3A4 in a concentration-dependent fashion (A, C), but the degree of activation for the truncated hemoprotein is considerably higher (B, D).

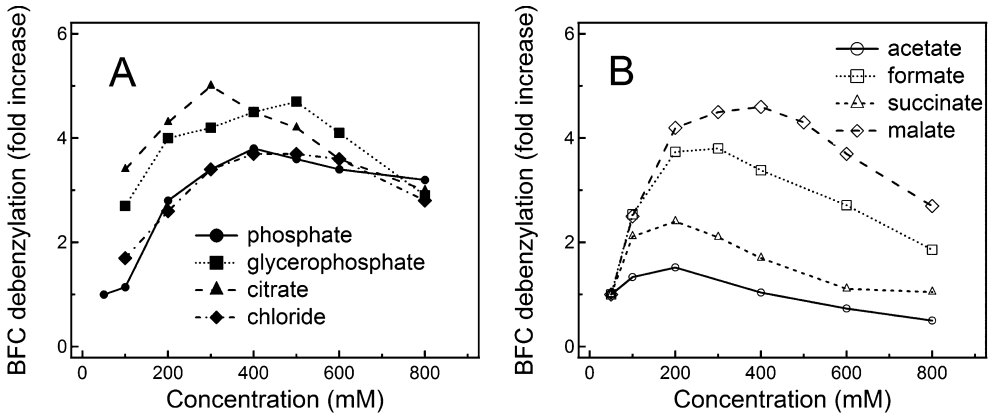

Figure 5. Relative impact of natural anionic compounds and NaCl on the BFC debenzylation activity of CYP3A4.

have similar ionic strengths. However, there were notable differences in the CYP3A4 activity vs [anion] plots determined for the similarly charged pairs: phosphate/glycerophosphate (Figure 5A), malate/succinate, and acetate/formate (Figure 5B). Given the lack of correlation between the ionic strength and a compound's effect on the BFC metabolism, it can be concluded that anions act in a structure-dependent manner and, in addition to the ionic strength-mediated effects (e.g., dehydration of the active site and strengthening of hydrophobic interactions), could stimulate CYP3A4 catalysis via specific anion−protein interactions. For instance, anions could bind to active site residues, controlling heme access, such as Arg212 and Ser119. To better understand the mechanism underlying the anion-dependent activation of CYP3A4, we investigated how citrate influences substrate binding and electron transfer to CYP3A4.

Citrate Promotes Substrate Binding to CYP3A4. Substrate binding is the first step in the CYP3A4 catalytic cycle (Figure 3) and, as we found, is strongly influenced by anions. Spectral measurements showed that citrate promotes the substrate-induced low-to-high spin shift in the heme iron in a concentration- and CYP3A4-form-dependent fashion (Figure 6A,B). In the presence of 100 μM TST, for instance, the high spin content in WT and trCYP3A4 increased from 60 to 80% and 45 to 80%, respectively, when the citrate concentration was elevated from 0 to 600 mM. A low-to-high spin transition also

DOI: 10.1021/acs.biochem.5b00510
Biochemistry 2015, 54, 4083−4096

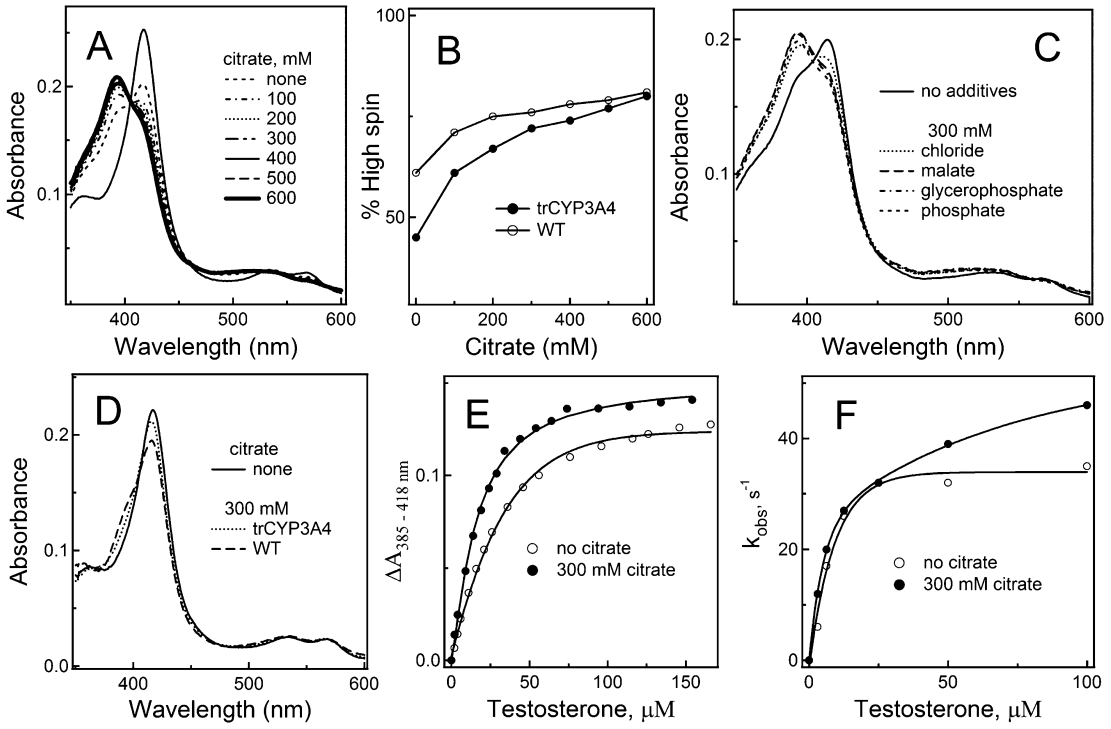

Figure 6. Effect of citrate and other anions on substrate binding to CYP3A4. (A, B) Spectral changes and the high spin content in CYP3A4, respectively, measured in the presence of 100 μM TST and various citrate concentrations. (C) Anion-dependent spectral changes in CYP3A4 recorded in the presence of 100 μM TST. (D) Citrate-dependent increase in the low-to-high spin transition observed in the presence of 50 μM BFC. (E) Dependence of absorbance changes in CYP3A4 on the TST concentration. Absorbance changes were determined during equilibrium titrations conducted in the absence and presence of 300 mM citrate. The TST concentration producing half occupation (S_{50}) and the Hill coefficient (n_H) derived from the titration plots are given in Table 1. Spectral experiments depicted in panels A–E were performed on 2–2.5 μM CYP3A4 in 100 mM phosphate, pH 7.4, at ambient temperatures. (F) Dependence of the observed rate constant (k_{obs}) for the CYP3A4–TST binding reaction on TST concentration. The k_{obs} values were determined at 23 °C by stopped-flow spectrophotometry. Interaction of CYP3A4 with TST in the absence and presence of 300 mM citrate was followed at 418 nm. Kinetic dissociation constants (K_d) and limiting rate constants (k_{lim}) derived from the plots are listed in Table 1.

was measured and found to be enhanced in the presence of phosphate, glycerophosphate, malate, and, to a lesser degree, NaCl (Figure 6C). Owing to limited amounts of BFC, spectral measurements were performed at fixed BFC and citrate concentrations (50 μM and 300 mM, respectively). As shown in Figure 6D, a BFC-dependent high spin transition, virtually undetectable in WT and trCYP3A4, was increased to 20 and 7%, respectively, upon addition of 300 mM citrate (Figure 6D). Thus, the CYP3A4–substrate binding process is affected by the N-terminal peptide and is greatly promoted by the anionic compounds.

Equilibrium titrations of WT CYP3A4 with TST showed that citrate does not perturb the sigmoidal character of the absorbance change vs [TST] plot, and leads to a slight decrease in the Hill coefficient (n_H of 1.2 vs 1.3 in the absence of citrate) and a 2-fold decrease in the TST concentration producing half occupation (S_{50} of 15 vs 28 μM in the absence of citrate; Figure 6E). Stopped-flow measurements, in turn, demonstrated that citrate does not alter the binding rate constant (k_{obs}) at TST concentrations ≤25 μM but elevates the k_{obs} value by ~20% at saturating TST (Figure 6F). A kinetic dissociation constant (K_d) calculated from the k_{obs} vs [TST] plot was in the same range as S_{50} and changed only slightly in the presence of citrate (Table 1). CYP3A4 is known to accommodate up to three TST molecules in the active site, where only the second TST binding leads to a detectable spin shift.[24] Our data suggest that citrate has no effect on the association of the first substrate but promotes binding of the second and, possibly, third TST molecule with no significant effect on the binding cooperativity.

Table 1. Effect of Citrate on the CYP3A4–TST Binding Reaction

	citrate	
	none	300 mM
high spin (%)[a]	52 ± 3	66 ± 2
S_{50} (μM)[b]	28 ± 4	15 ± 3
n_H[c]	1.2	1.3
K_d (μM)	8.4 ± 0.5	10.4 ± 0.7
k_{lim} (s^{-1})[d]	39 ± 4	48 ± 5

[a]TST concentration producing half occupation. [b]Hill coefficient. [c]Determined in the presence of 100 μM TST. [d]Limiting rate constant for the CYP3A4–TST binding reaction.

Effect of Citrate on CYP3A4 Reduction Kinetics. P450–substrate association is followed by a transfer of the first electron from CPR, which can be monitored by observing the Fe^{2+}-CO adduct formation. This process can be affected by a variety of factors, such as buffer composition, lipid environment, P450/CPR ratio, and the presence of substrate and cytochrome b_5.[25−27] We investigated kinetics of CYP3A4 reduction with equimolar CPR at 23 °C in the absence and presence of citrate. Reaction was initiated by injecting NADPH into a preincubated protein mixture (Figure 7) or by mixing

DOI: 10.1021/acs.biochem.5b00510
Biochemistry 2015, 54, 4083−4096

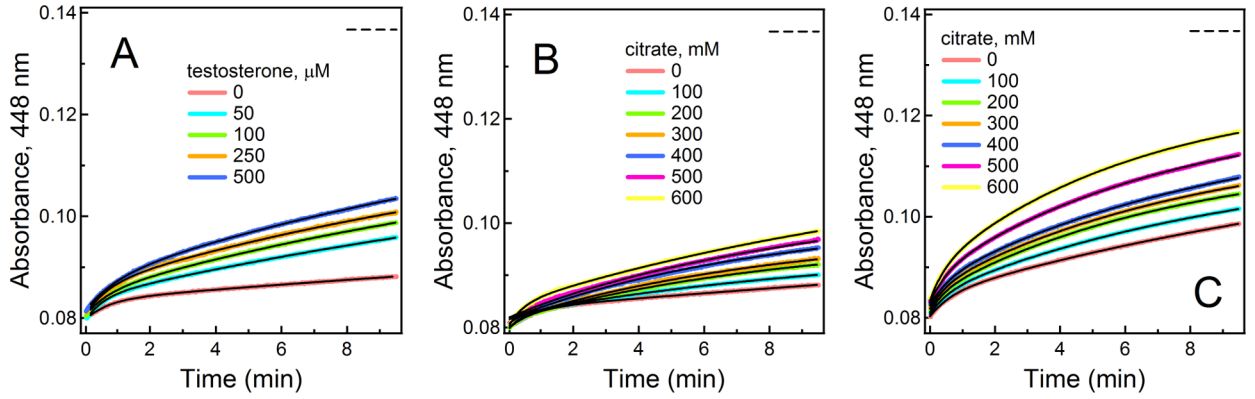

Figure 7. Kinetics of CYP3A4 reduction by CPR. Formation of the ferrous CYP3A4−CO adduct was monitored under anaerobic conditions at 23 °C and 448 nm. The reaction was initiated by injecting 100 μM NADPH to a preincubated mixture of CYP3A4 and CPR (1 μM each) in a sealed anaerobic cuvette. (A) Traces were recorded in 100 mM phosphate in the absence of citrate. (B, C) Traces were recorded in the absence and presence of 100 μM TST, respectively, at various citrate concentrations. Dashed lines show a 100% reduction level. Kinetics determined under all conditions were biphasic; double exponential fits are shown as black solid lines. The derived kinetic parameters, as well as the amount of a high spin form and CYP3A4 reduced during the fast phase and at the end of the reaction, are given in Table 3.

Table 2. Kinetic Parameters for the First Electron Transfer to CYP3A4 from CPR

	k_{fast} (min^{-1})	k_{slow} (min^{-1})	total Fe^{2+} (%)[a]	high spin (%)
no citrate				
testosterone, μM				
0	1.3 (5%)[b]	4.7×10^{-2}	14	0
50	1.9 (12%)	11.4×10^{-2}	28	34
100	1.6 (12%)	12.0×10^{-2}	33	52
250	1.5 (14%)	13.8×10^{-2}	38	64
500	1.5 (15%)	15.6×10^{-2}	41	70
no testosterone				
citrate, mM				
0	1.3 (5%)	4.7×10^{-2}	14	0
100	1.8 (11%)	6.8×10^{-2}	18	4
200	1.9 (11%)	8.8×10^{-2}	21	4
300	1.8 (11%)	9.5×10^{-2}	23	4
400	1.5 (9%)	11.4×10^{-2}	27	4
500	1.4 (8%)	12.6×10^{-2}	30	4
600	1.2 (8%)	13.1×10^{-2}	32	4
100 μM testosterone				
citrate, mM				
0	1.6 (11%)	12.0×10^{-2}	33	52
100	1.9 (12%)	12.8×10^{-2}	38	56
200	2.4 (13%)	13.2×10^{-2}	43	62
300	2.3 (13%)	14.3×10^{-2}	46	66
400	2.2 (12%)	15.3×10^{-2}	49	68
500	2.2 (12%)	15.9×10^{-2}	57	71
600	2.2 (11%)	16.5×10^{-2}	65	73

[a]Fraction of CYP3A4 reduced during the entire course of the reaction. [b]Percentage of absorbance changes observed during the fast phase.

CYP3A4 with the NADPH-reduced CPR (Supporting Information Figure S1). The kinetics were biphasic under all studied conditions, with no dependency of the rate constant for the fast phase (k_{fast}) on [TST] and the content of the high spin form. In contrast, the rate constants for the slow phase (k_{slow}) and the fraction of CYP3A4 reduced in the fast phase (%k_{fast}) and at the end of the reaction were TST- and citrate-dependent (Table 2). Despite differences in the assay conditions, our results agree with the kinetic data obtained on the lipid-bound Δ3−12 CYP3A4, reduction of which was also substrate-independent and proceeded with a similar rate, <2 min^{-1}.[26] One notable difference was that, in our reconstituted system, the order of CYP3A4 and CPR mixing had only a weak effect on the electron transfer rate (~10−25% decrease in all kinetic parameters), meaning that preincubation of soluble CYP3A4 and CPR only slightly promotes their complex formation. Nonetheless, taken together, our and previously reported results indicate that the CPR-to-CYP3A4 electron transfer is governed by factors other than the spin transition and, in part, could be limited by a slow CYP3A4−CPR association process.

Citrate Accelerates Kinetics of CPR Reduction with NADPH. Since electron exchange between CPR and CYP3A4 can be controlled by the properties of both redox partners, we next investigated how citrate affects the function of CPR.

DOI: 10.1021/acs.biochem.5b00510
Biochemistry 2015, 54, 4083−4096

Mammalian CPR is a complex and highly charged molecule consisting of four structural domains: the N-terminal transmembrane fragment, FAD/NADP(H)- and FMN-binding domains, and a connecting module that allows reorientation of the flavin domains.[28] Through domain−domain interaction, CPR could control the accessibility and redox state of FMN (an electron donor to P450) and, subsequently, the outcome of the CYP3A4 catalytic cycle.

We analyzed the effect of citrate on the reaction of CPR with NADPH, the source of electrons for the mammalian P450-dependent monooxygenase systems. This reaction has been investigated by various techniques,[29−39] which helped to establish the direction of electron flow and identify transient and catalytically competent redox intermediates in CPR (shown in Figure 8). Due to the complexity of the NADPH/CPR

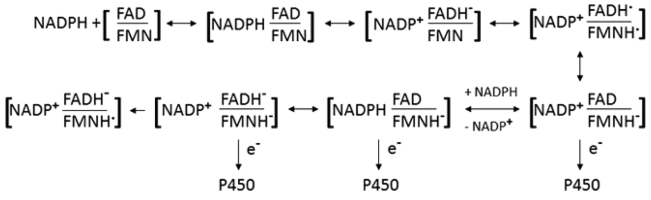

Figure 8. Intermediates formed during reduction of CPR with NADPH, according to previous investigations.[29−39] The binding of NADPH to CPR results in production of the NADPH−FAD charge transfer complex, which is followed by a two-electron reduction of FAD and formation of the $NADP^+$−$FADH^-$ charge-transfer complex. Both types of the charge-transfer complex absorb in the long-wavelength region. The next step is interflavin electron transfer, leading to accumulation of the $FADH^•$ and $FMNH^•$ semiquinone species with a characteristic peak at 550−650 nm and, subsequently, the two-electron reduction of FMN. If the reductant is present in excess, then CPR can bind the second NADPH molecule and become fully reduced. Only intermediates with the two-electron reduced FMN are catalytically competent and can donate electrons to P450. In the absence of an electron acceptor, the three-electron reduced forms accumulate in anaerobic solutions because the fully reduced CPR is thermodynamically unstable.

oxidoreduction process, we attempted to determine a general trend in the kinetic changes rather than define the effect of citrate on the individual reaction steps. Using a stopped-flow spectrophotometer, spectral perturbations were recorded under anaerobic conditions at 3 °C and within 100 s after mixing CPR with a 10-fold excess of NADPH. Both diode array scans and single-wavelength kinetic data were collected and analyzed. The FAD and FMN reduction, accumulation of flavin semiquinones, and formation of the charge-transfer complex between the FAD and pyridine cofactor were followed at 456, 600, and 730 nm, respectively. On the basis of the spectral changes, we identified three main reaction phases and six consecutive kinetic steps with the rate constants of 18, 9, 0.6, 0.13, 0.018, and 0.004 s^{-1} (Figure 9, Table 3). The first and fastest phase reflects the NADPH binding and two-electron reduction of FAD, leading to the $NADP^+$−$FADH^-$ charge-transfer complex formation and the first rise in the 730 nm absorbance. The interflavin electron transfer and binding of the second NADPH molecule occur during the second phase, characterized by a decrease and the second spike in the 730 nm absorbance. Disproportionation and thermodynamic equilibration between the fully and partially reduced forms most likely take place during the slow third phase.

Citrate was found to promote the NADPH-induced CPR reduction in a concentration-dependent manner. The rate constants for all kinetic steps were increased by ∼2−4-fold at 300−400 mM citrate and remained unchanged or slightly decreased at higher anion concentrations (Table 3). Since the citrate-dependent stimulation of the first reductive step (NADPH−FAD → $NADP^+$−$FADH^-$) could affect all consecutive electron transfer steps, it is not possible to conclude which reactions beside FAD reduction are affected by citrate and to what extent. Even so, it is evident from the kinetic data that citrate markedly accelerates the CPR−NADPH interaction and interflavin electron exchange, which, in turn, could translate to a higher steady-state turnover of CPR.

Considering the flavin reduction kinetics and the maximal turnover of our reconstituted system (∼4 min^{-1} at 37 °C; Figure 4C), we suggest that the [$NADP^+$, $FADH^-$, $FMNH^-$] and [$NADP^+$(H), $FADH^•$, FMN^-] intermediates, whose formation rate is projected to reach 6−20 min^{-1} at 37 °C, most likely serve as electron donors to CYP3A4 during catalysis. The same species could also be responsible for heme reduction during the fast phase of the CPR-to-CYP3A4 electron transfer reaction (k_{fast} of 1.2−2.4 min^{-1} at 23 °C; Table 2). In the presence of a large excess of NADPH, the [FAD, $FMNH^-$] and [NADPH, FAD, $FMNH^-$] species will be produced too fast (projected rate of 220−800 min^{-1} at 37 °C) and, thus, they could undergo further reduction or disproportionation before productive collisions with CYP3A4 occur. In contrast, the slow phase in the electron transfer reaction is likely mediated by the thermodynamically stable [$NADP^+$, $FADH^-$, $FMN^•$] species, expected to predominate in solutions 2−10 min after addition of NADPH.

Effect of Citrate on the Steady-State Redox Activities of CPR. As the kinetic data predicted, the steady-state turnover for the CPR-catalyzed NADPH oxidation was enhanced up to 2−2.5-fold at high citrate concentrations (Figure 10A). Most interestingly, the effect of citrate was more pronounced when WT or trCYP3A4 was present in the reaction mixture. Simultaneous addition of equimolar WT CYP3A4 and high citrate concentrations led to a maximal (∼5.5-fold) increase in the NADPH oxidase activity. Since NADPH oxidation was measured in the absence of CYP3A4 substrates and k_{fast} for the reduction of ligand-free CYP3A4 is virtually citrate-independent (Table 2), such a drastic stimulation was not due to an increased CPR-to-CYP3A4 electron flow. One possible scenario is that citrate modulates the redox properties of CPR both solely and through CPR−CYP3A4 interaction.

Reduction of cytochrome *c*, which accepts electrons from the FMN moiety of CPR, was promoted by citrate and other anions as well. The relative impact of various compounds (at 300 mM) on the NADPH oxidase and cytochrome *c* reductase activities of the full-length and trCPR is compared in Figure 10B. The activity profiles for the two CPR forms are identical, which allows us to conclude that anions act on the catalytic rather than N-terminal domain, strictly required for the reduction of mammalian P450s.[40−42]

Effect of Anions on Flavin Fluorescence in CPR. To gain further insights into the mechanism of anion-dependent stimulation of the redox function of CPR, we investigated changes in flavin fluorescence. The FAD group in CPR is buried and does not emit light upon excitation. The fluorescence yield of loosely bound FMN, on the other hand, depends on the CPR conformation and is expected to increase in the catalytically competent "open" conformation due to a

DOI: 10.1021/acs.biochem.5b00510
Biochemistry 2015, 54, 4083−4096

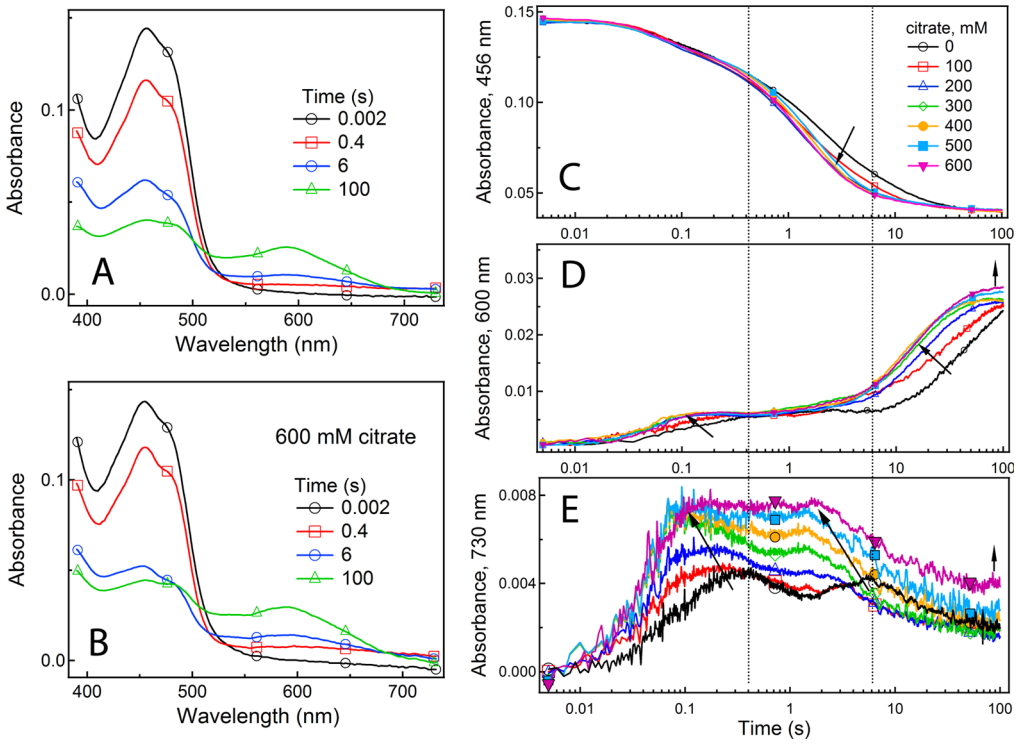

Figure 9. Effect of citrate on the reduction of CPR with NADPH. Spectral perturbations were recorded at 3 °C in a stopped-flow spectrophotometer as described in the Experimental Procedures. Both diode array spectra (A, B) and single-wavelength kinetics (C–E) were recorded as a function of logarithmic time. The FAD and FMN reduction, formation of the flavin semiquinone forms, and production of the $NADP^+$–$FADH^-$ charge-transfer complex were monitored at 456, 600, and 730 nm, respectively. Three phases (separated by vertical dotted lines) and six consecutive reductive steps were detected within the 100 s time course. Spectra recorded at the end of each phase in the absence and presence of 600 mM citrate are shown in plots A and B, respectively. Rate constants derived from the single-wavelength kinetics, as well as intermediates likely formed during each phase are shown in Table 3. Citrate promotes all reductive steps in a concentration-dependent manner and shifts the reaction course, as indicated by arrows in panels C–E.

Table 3. Effect of Citrate on the Kinetics of CPR Reduction with NADPH

	reaction phase and redox intermediates					
	I		II		III	
			[$FADH^•$, $FMNH^•$]		[$NADP^+$, $FADH^-$, $FMNH^-$][a]	
			[FAD, $FMNH^-$]		[$NADP^+$(H), $FADH^•$, FMN^-][a]	
	[$NADP^+$, $FADH^-$, FMN]		[NADPH, FAD, $FMNH^-$]		[$NADP^+$, $FADH^-$, $FMN^•$]	
		k (s^{-1})				
citrate, mM					[a]	
0	18	9	0.6	0.13	0.018	0.004
100	32	11	0.9	0.19	0.026	0.004
200	40	17	1.5	0.36	0.035	0.007
300	50	20	2.3	0.84	0.049	0.007
400	52	20	1.5	0.73	0.055	0.008
500	54	20	1.3	0.63	0.049	0.006
600	52	20	1.3	0.60	0.049	0.005

[a]Catalytically competent intermediates and their formation rates.

larger exposure of the FMN. None of the investigated anionic compounds significantly perturbed the fluorescent yield of free FMN. The CPR fluorescence, however, was increased by 3-fold in the presence of glycerophosphate and to a lesser degree (<1.8-fold) in the presence of other compounds (Figure 10C). A stronger effect of glycerophosphate could be due to its structural resemblance to the phospho-ribitol portion of FMN and, hence, a potential ability to occupy the phosphate-binding site in the FMN domain, which may lead to partial FMN dissociation. CYP3A4 also did not change the fluorescence of free FMN but quenched CPR fluorescence by ~2-fold regardless of the anion type present in solution (Figure 10C). In the absence of anions, addition of equimolar CYP3A4 leads only to negligible changes in the CPR emission (~7% decrease). These findings suggest that citrate and other anions could induce reorientation of the flavin domains and facilitate CPR–CYP3A4 complex formation.

Effect of Citrate on the Oligomeric State of CYP3A4 and CPR. To elucidate whether citrate promotes formation of long-lived CYP3A4–CPR complexes, we determined the molecular weight of CYP3A4 and CPR individually and in an equimolar mixture. Gel filtration experiments showed that citrate has no effect on the oligomeric state of isolated CYP3A4 and CPR and does not lead to the formation of their long-lived complexes (Figure 11). trCYP3A4 eluted as a dimer, whereas full-length CYP3A4 formed aggregates with an average molecular weight of ~280 kDa, corresponding to a tetramer. These aggregates did not dissociate in the presence of 300 mM citrate, PRG, or equimolar CPR. CPR, on the other hand, formed higher-order oligomers that partially dissociated in the presence of CYP3A4 (from ~750 to 550 kDa; Figure 11). Thus, one mechanism through which CYP3A4 could stimulate the activity of CPR is by promoting its disaggregation. Heterogeneity and a different oligomeric state of WT and trCYP3A4, in turn, could explain functional differences between

DOI: 10.1021/acs.biochem.5b00510
Biochemistry 2015, 54, 4083–4096

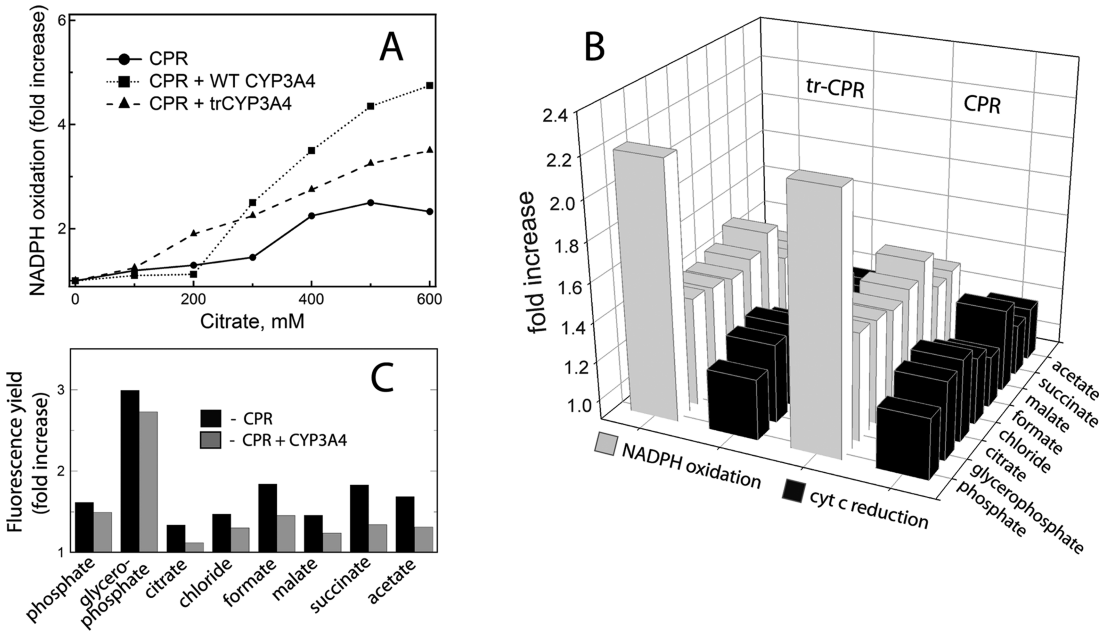

Figure 10. Effect of citrate and other anions on the redox activity and fluorescence of CPR. All measurements were conducted at 23 °C in 50 mM phosphate, pH 7.4. (A) NADPH oxidase activity measured at various citrate concentrations and in the absence and presence of equimolar WT and trCYP3A4. (B) Relative impact of anionic compounds on the NADPH oxidase and cytochrome *c* reductase activities of WT and trCPR. (C) Anion- and CYP3A4-dependent changes in the flavin fluorescence of CPR. The anion concentration was 300 mM; excitation and emission wavelengths were 450 and 520 nm, respectively.

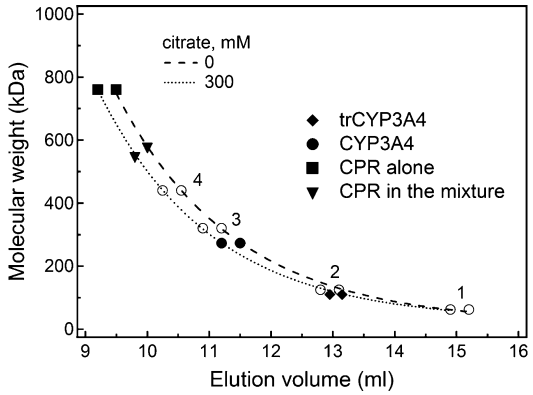

Figure 11. Effect of citrate on the oligomeric state of CYP3A4 and CPR. Calibration curves and molecular weight of WT CYP3A4 and CPR alone and in their equimolar mixtures were determined in the absence and presence of 300 mM citrate. Molecular standards used are as follows: 1 and 2, oxidized monomer (62 kDa) and NADH-reduced dimer of apoptosis inducing factor (125 kDa), respectively; 3, nitric oxide synthase (320 kDa); and 4, ferritin (440 kDa).

the two forms (Figure 4) and biphasicity in the heme reduction kinetics (Figure 7).

DISCUSSION

Peripheral Site Might Be Predisposed to Progesterone Binding. The existence of multiple substrate-binding sites in CYP3A4 was proposed nearly 2 decades ago,[3,43] whereas more recent studies suggested that the substrate/effector molecules could cooperatively associate not only within but also outside the active site cavity.[12,44,45] Direct evidence for the existence of a peripheral ligand-binding site was provided by Williams et al.,[8] who co-crystallized CYP3A4 with PRG bound on a surface 17 Å away from the catalytic site. Based on this structure and mutagenesis data,[8,12] the PRG docking area was proposed to be functionally important and serve as a substrate/effector-binding site. There are some facts, however, that do not support this suggestion.

For example, Williams and co-workers did not mention that the peripheral site is located at the crystallographic interface and that the PRG-binding mode is stabilized via contacts with the symmetry-related PRG and CYP3A4 molecules (Figure 1C,D). Without these interactions, the surface cleft would be too shallow for the binding/retaining of PRG and other molecules of a similar or larger size. For instance, in addition to PRG, CYP3A4 metabolizes TST, androstenedione, and cholesterol, but none of these structurally similar compounds binds to the peripheral site during crystallization (our trials). Computer modeling showed (Supporting Information Figure S2) that steric clashing imposed by the elongated side chain of cholesterol may prevent or weaken its association to the PRG site, whereas TST and androstenedione fit well but cannot establish a hydrogen bond with Asp214 that stabilizes the CYP3A4−PRG complex.

Further, molecular dynamics (MD) simulations were performed on monomeric nanodisc-incorporated CYP3A4, where the peripheral site is partially embedded into the membrane. During the 100 ns MD simulation, PRG remained bound and maintained hydrophobic contacts with the surrounding residues, whereas carbamazepine, another midsize hydrophobic substrate of CYP3A4, became detached from the peripheral site in three out of four independent MD simulations.[46] This implies that association of the F′-G′ peptide with the lipid bilayer may be a prerequisite for the substrate/effector attachment to the peripheral cleft. It remains to be elucidated, though, whether other structurally diverse effector molecules (e.g., α-naphthoflavone, Nile Red, aflatoxin, and others) can dock to the peripheral area and remain bound during catalytic turnover. Even if they do, it is unclear how their

DOI: 10.1021/acs.biochem.5b00510
Biochemistry 2015, 54, 4083−4096

association could affect metabolism of substrates present in the active site because PRG does not induce any notable changes in the CYP3A4 X-ray structure. The only change detected during MD simulations on CYP3A4[46] was a transient reorientation of the Phe213 side chain, pointing toward the heme in substrate-free CYP3A4 and flipping out upon PRG binding. This conformational switch was proposed to mediate heterotropic cooperativity in CYP3A4 because it leads to a ~300 Å^2 increase in the active site volume, thereby allowing substrates to bind closer to the heme and undergo oxidation. It has not been tested, however, whether the L211F/D214E mutation, famously known to perturb both homotropic and heterotropic cooperativity in CYP3A4 *in vitro*,[12] has any effect on the manner of PRG association and conformation of Phe213.

F′-G′-Mediated Dimerization of CYP3A4 Prevents Bitopic Membrane Insertion. In addition to the transmembrane N-terminal tail, mammalian P450s are predicted to interact with the lipid bilayer through the peptides comprising the substrate access channel that correspond to the B-C and F′-G′ fragments in CYP3A4.[10,11,47−53] Such an arrangement could help to partition/translocate lipophilic compounds from the membrane into the substrate access channel and further to the P450 active site. So far, the crystal structure only for the truncated CYP3A4 has been determined, which also associates with bacterial membranes during heterologous expression and requires detergents for solubilization. Since detergents are removed during purification, the most hydrophobic area in the CYP3A4 catalytic domain, the F′-G′ peptide, has a greater tendency to aggregate in aqueous solutions than other surface areas. This could lead to the nonspecific dimerization observed in the crystal lattice and detected by size exclusion chromatography (Figure 11) and chemical cross-linking.[54] A possible tetrametic organization (a dimer of dimers) can be seen in the 2VOM and 4K9W structures,[6,7] containing four CYP3A4 molecules per asymmetric unit.

It needs to be emphasized that crystallographic tetramers are incompatible with the membrane topology of CYP3A4, whereas crystallographic dimers could be inserted into the lipid bilayer only monotopically through the N-termini. Further, in contrast to the bitopically incorporated monomeric form, the interlocked F′-G′ regions in CYP3A4 dimers would not be able to reach and partition lipophilic substrates from the membrane. Most importantly, CYP3A4 dimers would have a restricted motional freedom critical for accommodation and release of large-size substrates and products (compare Figures 1C and 2A), which, in turn, would have a negative effect on metabolism. Thus, the functional relevance of the crystallographic dimer and the symmetry-related PRG molecules trapped at the dimer interface is questionable.

Nonetheless, the biological relevance of the dimeric form of CYP3A4 has been recently suggested.[54,55] Using membraneous reconstituted systems with different lipid/protein ratios, Davydov and co-workers investigated how the degree of CYP3A4 oligomerization, varied by increasing or decreasing the enzyme concentration, changes the activating effect of α-naphthoflavone on the BFC debenzylation reaction.[55] The extent of CYP3A4 oligomerization was concluded to directly contribute to its complex allosteric behavior and could modulate the effector role of α-naphthoflavone. Most recently, the same group proposed a trimeric organization of membrane-bound CYP3A4 and suggested that its catalytic properties could be altered upon formation of hetero-oligomers with other P450 isoforms.[54] In both studies, a Δ3−12 construct of CYP3A4 was utilized, with no proof provided whether the truncated form has the same membrane topology as WT. Furthermore, results on the relationship between α-naphthoflavone's activating effect and CYP3A4 oligomerization could not be reproduced in membraneous systems containing WT CYP3A4.[55] Functional data on nanodisc-incorporated CYP3A4, on the other hand, provided compelling evidence that the P450 monomers undergo activation and display cooperative effects in a manner similar to that of the native microsomal protein.[46] Thus, the relevance and impact of oligomerization on the CYP3A4 function needs to be further and more carefully examined.

Anion-Dependent Activation of CYP3A4 Monooxygenase. It has been long known that CYP3A4 requires negatively charged phospholipids, such as phosphatidylserine and phosphatidic acid, for membrane incorporation, efficient catalytic activity, and interaction with CPR.[20−22] A negative membrane potential was proposed to facilitate disaggregation and proper positioning of CYP3A4 via complementary charge−charge interactions.[22] These interactions could be mediated by Lys34 and Lys35 from the N-terminal A″-helix, a unique structural element in CYP3A4 (Figure 2A, B). In addition to anionic phospholipids, high phosphate concentrations were reported to stimulate the catalytic activity of CYP3A4 (formerly known as P-450p and P450IIIA1) but not two other mammalian P450 isoforms, which was attributed to the ionic strength-dependent changes in the redox partner interaction.[23] Comprehensive investigations on electron transfer between CPR and various mammalian P450s[56−59] showed that, indeed, heme reduction was enhanced at high ionic strength, leading to the conclusion that hydrophobic interactions rather than charge pairing play a leading role in P450−CPR complex formation.

This study unravels the complexity of the ionic strength/anion-dependent effects and suggests that acceleration of the interprotein electron transfer at high salt concentrations may result from a chain of events preceding CPR−P450 complex formation and electron exchange. Comparative analysis of the citrate-dependent changes in the metabolism of BFC and TST (Figures 4 and 5), substrate binding (Figure 6), CPR-to-CYP3A4 electron transfer (Figure 7), and redox and molecular properties of CPR (Figures 9-11) allowed us to conclude that citrate and other anions (i) stimulate CYP3A4 catalysis in a concentration-, structure-, and CYP3A4-form-dependent manner and exert their action not only through changes in ionic strength but also via specific protein-anion interactions; (ii) facilitate CYP3A4−substrate complex formation by increasing the binding rate, affinity, and low-to-high spin transition in the heme iron; (iii) promote the CPR-to-CYP3A4 electron transfer by accelerating reduction of CPR with NADPH; and (iv) optimize the CYP3A4−CPR interaction through the flavin domain orientation and disaggregation of CPR.

We did not investigate how citrate affects the last three steps in the CYP3A4 cycle: oxygen binding, the second electron transfer, and product release (Figure 3). Oxygen binding to ferrous P450 is a diffusion-controlled process limited by the rate of the heme reduction, whereas the second electron transfer to the ferrous O_2-bound form depends on the availability of the $FMNH^-$ species in CPR. Thus, formation and reduction of the ferrous CYP3A4−O_2 complex are expected to follow the trend deduced from the preceding reactions and increase at high citrate concentrations. Product release, however, may be negatively affected by an increase in ionic strength because the TST and BFC metabolites are hydrophobic molecules and their dissociation from the

DOI: 10.1021/acs.biochem.5b00510
Biochemistry 2015, 54, 4083−4096

CYP3A4 active site could be impeded at high anion concentrations. This possibility explains the bell-shaped dependencies of the CYP3A4 activity vs anion concentration (Figures 4A,C and 5), as well as the higher extent of activation for the BFC debenzylation reaction (Figure 4). HFC is less hydrophobic than hydroxy-TST and, hence, its egress is likely to be less affected at high ionic strength.

Finally, our findings provide a mechanistic explanation for the stimulating effect of high phosphate concentrations on lipid-bound CYP3A4,[23,60,61] help to better understand why CYP3A4 activity is greatly affected by the assay conditions[26,27] (and references therein), and also suggest how the activity assays, widely used to predict metabolism of drugs in humans, can be improved. According to our study, addition of 100−300 mM phosphate, citrate, or malate to the assay buffer could markedly increase CYP3A4 turnover without affecting the product profile. Although *in vitro* activation of CYP3A4 monooxygenase takes place at anion concentrations greatly exceeding their physiological levels, a cumulative action of intracellular phosphate, glycerophosphate, and di- and tricarboxylic acids on CPR and CYP3A4 is possible and could affect *in vivo* drug metabolism.

CONCLUSIONS

Our crystallization trials and analysis of the CYP3A4−PRG complex structure suggest that the surface cleft above the phenylalanine cluster might be predisposed to PRG binding. A novel anion-binding site occupied by citrate was observed in one of the newly determined CYP3A4−PRG structures. This site is positioned suitably for interaction with the negatively charged head groups of the membrane phospholipids, although its functional role in membrane-bound CYP3A4 remains to be established. In solution, citrate was found to stimulate catalysis of CYP3A4 via a complex mechanism, mostly affecting the CYP3A4−substrate binding step, reaction of CPR with NADPH, and interflavin and interprotein electron transfer. Comparative analysis of various negatively charged organic compounds indicates that anions act on the catalytic domains of CYP3A4 and CPR in a structure-dependent manner and, hence, in addition to alterations caused by changes in ionic strength, could modulate the properties of both redox partners through specific anion−protein interactions. Together, our results demonstrate that the outcome of the CYP3A4 monooxygenase reaction conducted under different ionic strengths and buffer compositions is defined by the action of specific ions on the individual properties of CYP3A4 and CPR, as well as on the redox partner interaction. Given the complexity of the anion-induced effects, interpretation and comparison of experimental data obtained under different ionic strengths and buffer compositions should be done with caution.

ASSOCIATED CONTENT

Supporting Information

Data collection and refinement statistics; kinetics of CYP3A4 reduction in the presence of TST upon mixing with the NADPH-reduced CPR; and a view at the peripheral PRG-binding site in CYP3A4 with the superimposed cholesterol, testosterone, and androstenedione molecules. The Supporting Information is available free of charge on the ACS Publications website at DOI: 10.1021/acs.biochem.5b00510.

AUTHOR INFORMATION

Corresponding Author

*Tel: (949) 824-1953; E-mail: sevrioui@uci.edu.

Funding

This work was supported by National Institutes of Health Grant GM57353.

Notes

The authors declare no competing financial interest.

ACKNOWLEDGMENTS

This work involves research carried out at the Advanced Light Source and the Stanford Synchrotron Radiation Lightsource, a national user facility operated by Stanford University on behalf of the U.S. Department of Energy, Office of Basic Energy Sciences. The Advanced Light Source is supported by the Director, Office of Science, Office of Basic Energy Sciences, of the U.S. Department of Energy under contract no. DE-AC02-05CH11231. The SSRL Structural Molecular Biology Program is supported by the Department of Energy, Office of Biological and Environmental Research, and by the National Institutes of Health, National Center for Research Resources, Biomedical Technology Program, and the National Institute of General Medical Sciences. The authors thank B. Berhane for assistance with the mass spectrometry measurements.

ABBREVIATIONS

CYP3A4, 3A4 isoform of cytochrome P450; trCYP3A4, a truncated, membrane linker-free form of CYP3A4; CPR, cytochrome P450 reductase; trCPR, a truncated, membrane linker-free form of CPR; BFC, 7-benzyloxy-4-(trifluoromethyl)-coumarin; HFC, 7-hydroxy-4-trifluoromethylcoumarin; PRG, progesterone; TST, testosterone; WT, wild type

REFERENCES

(1) Guengerich, F. P. (1999) Cytochrome P-450 3A4: regulation and role in drug metabolism. *Annu. Rev. Pharmacol. Toxicol. 39*, 1−17.

(2) Wienkers, L. C., and Heath, T. G. (2005) Predicting *in vivo* drug interactions from *in vitro* drug discovery data. *Nat. Rev. Drug Discovery 4*, 825−833.

(3) Ueng, Y. F., Kuwabara, T., Chun, Y. J., and Guengerich, F. P. (1997) Cooperativity in oxidations catalyzed by cytochrome P450 3A4. *Biochemistry 36*, 370−381.

(4) Atkins, W. M., Wang, R. W., and Lu, A. Y. (2001) Allosteric behavior in cytochrome P450-dependent *in vitro* drug−drug interactions: a prospective based on conformational dynamics. *Chem. Res. Toxicol. 14*, 338−347.

(5) Hutzler, J. M., and Tracy, T. S. (2002) Atypical kinetic profiles in drug metabolism reactions. *Drug. Metab. Dispos. 30*, 355−362.

(6) Ekroos, M., and Sjogren, T. (2006) Structural basis for ligand promiscuity in cytochrome P450 3A4. *Proc. Natl. Acad. Sci. U.S.A. 103*, 13682−13687.

(7) Sevrioukova, I. F., and Poulos, T. L. (2013) Dissecting cytochrome P450 3A4−ligand interactions using ritonavir analogues. *Biochemistry 52*, 4474−4481.

(8) Williams, P. A., Cosme, J., Vinkovic, D. M., Ward, A., Angove, H. C., Day, P. J., Vonrhein, C., Tickle, I. J., and Jhoti, H. (2004) Crystal structures of human cytochrome P450 3A4 bound to metyrapone and progesterone. *Science 305*, 683−686.

(9) Sevrioukova, I. F., and Poulos, T. L. (2012) Structural and mechanistic insights into the interaction of cytochrome P4503A4 with bromoergocryptine, a type I ligand. *J. Biol. Chem. 287*, 3510−3517.

(10) Zhao, Y., White, M. A., Muralidhara, B. K., Sun, L., Halpert, J. R., and Stout, C. D. (2006) Structure of microsomal cytochrome P450 2B4 complexed with the antifungal drug bifonazole: insight into P450

DOI: 10.1021/acs.biochem.5b00510
Biochemistry 2015, 54, 4083−4096

conformational plasticity and membrane interaction. *J. Biol. Chem. 281*, 5973−5981.
(11) Denisov, I. G., Shih, A. Y., and Sligar, S. G. (2012) Structural differences between soluble and membrane bound cytochrome P450s. *J. Inorg. Biochem. 108*, 150−158.
(12) Harlow, G. R., and Halpert, J. R. (1998) Analysis of human cytochrome P450 3A4 cooperativity: construction and characterization of a site-directed mutant that displays hyperbolic steroid hydroxylation kinetics. *Proc. Natl. Acad. Sci. U.S.A. 95*, 6636−6641.
(13) Sevrioukova, I. F., and Poulos, T. L. (2010) Structure and mechanism of the complex between cytochrome P4503A4 and ritonavir. *Proc. Natl. Acad. Sci. U.S.A. 107*, 18422−18427.
(14) Shen, A. L., Porter, T. D., Wilson, T. E., and Kasper, C. B. (1989) Structural analysis of the FMN binding domain of NADPH-cytochrome P-450 oxidoreductase by site-directed mutagenesis. *J. Biol. Chem. 264*, 7584−7589.
(15) Djordjevic, S., Roberts, D. L., Wang, M., Shea, T., Camitta, M. G., Masters, B. S., and Kim, J. J. (1995) Crystallization and preliminary X-ray studies of NADPH-cytochrome P450 reductase. *Proc. Natl. Acad. Sci. U.S.A. 92*, 3214−3218.
(16) Collaborative computational project number 4 (1994) The CCP4 suite programs for protein crystallography. *Acta Crystallogr., Sect. D: Biol. Crystallogr. 50*, 760−763.
(17) Emsley, P., Lohkamp, B., Scott, W. G., and Cowtan, K. (2010) Features and development of Coot. *Acta Crystallogr., Sect. D: Biol. Crystallogr. 66*, 486−501.
(18) Adams, P. D., Afonine, P. V., Bunkoczi, G., Chen, V. B., Davis, I. W., Echols, N., Headd, J. J., Hung, L. W., Kapral, G. J., Grosse-Kunstleve, R. W., McCoy, A. J., Moriarty, N. W., Oeffner, R., Read, R. J., Richardson, D. C., Richardson, J. S., Terwilliger, T. C., and Zwart, P. H. (2010) PHENIX: a comprehensive Python-based system for macromolecular structure solution. *Acta Crystallogr., Sect. D: Biol. Crystallogr. 66*, 213−221.
(19) Sohl, C. D., Cheng, Q., and Guengerich, F. P. (2009) Chromatographic assays of drug oxidation by human cytochrome P450 3A4. *Nat. Protoc. 4*, 1252−1257.
(20) Imaoka, S., Imai, Y., Shimada, T., and Funae, Y. (1992) Role of phospholipids in reconstituted cytochrome P450 3A form and mechanism of their activation of catalytic activity. *Biochemistry 31*, 6063−6069.
(21) Ingelman-Sundberg, M., Hagbjork, A. L., Ueng, Y. F., Yamazaki, H., and Guengerich, F. P. (1996) High rates of substrate hydroxylation by human cytochrome P450 3A4 in reconstituted membranous vesicles: influence of membrane charge. *Biochem. Biophys. Res. Commun. 221*, 318−322.
(22) Kim, K.-H., Aln, T., and Yun, C.-H. (2003) Membrane properties induced by anionic phospholipids and phosphatidylethanolamine are critical for the membrane binding and catalytic activity of human cytochrome P450 3A4. *Biochemistry 42*, 15377−15387.
(23) Gemzik, B., Halvorson, M. R., and Parkinson, A. (1990) Pronounced and differential effects of ionic strength and pH on testosterone oxidation by membrane-bound and purified forms of rat liver microsomal cytochrome P-450. *J. Steroid Biochem. 35*, 429−440.
(24) Denisov, I. G., Baas, B. J., Grinkova, Y. V., and Sligar, S. G. (2007) Cooperativity in cytochrome P450 3A4: linkages in substrate binding, spin state, uncoupling, and product formation. *J. Biol. Chem. 282*, 7066−7076.
(25) Yamazaki, H., Johnson, W. W., Ueng, Y. F., Shimada, T., and Guengerich, F. P. (1996) Lack of electron transfer from cytochrome *b*5 in stimulation of catalytic activities of cytochrome P450 3A4. Characterization of a reconstituted cytochrome P450 3A4/NADPH-cytochrome P450 reductase system and studies with apo-cytochrome b_5. *J. Biol. Chem. 271*, 27438−27444.
(26) Guengerich, F. P., and Johnson, W. W. (1997) Kinetics of ferric cytochrome P450 reduction by NADPH-cytochrome P450 reductase: rapid reduction in the absence of substrate and variations among cytochrome P450 systems. *Biochemistry 36*, 14741−14750.
(27) Farooq, Y., and Roberts, G. C. (2010) Kinetics of electron transfer between NADPH-cytochrome P450 reductase and cytochrome P450 3A4. *Biochem. J. 432*, 485−493.
(28) Wang, M., Roberts, D. L., Paschke, R., Shea, T. M., Masters, B. S., and Kim, J. J. (1997) Three-dimensional structure of NADPH-cytochrome P450 reductase: prototype for FMN- and FAD-containing enzymes. *Proc. Natl. Acad. Sci. U.S.A. 94*, 8411−8416.
(29) Masters, B. S., Bilimoria, M. H., Kamin, H., and Gibson, Q. H. (1965) The mechanism of 1- and 2-electron transfers catalyzed by reduced triphosphopyridine nucleotide-cytochrome c reductase. *J. Biol. Chem. 240*, 4081−4088.
(30) Masters, B. S., Kamin, H., Gibson, Q. H., and Williams, C. H., Jr. (1965) Studies on the mechanism of microsomal triphosphopyridine nucleotide-cytochrome *c* reductase. *J. Biol. Chem. 240*, 921−931.
(31) Iyanagi, T., Makino, N., and Mason, H. S. (1974) Redox properties of the reduced nicotinamide adenine dinucleotide phosphate-cytochrome P-450 and reduced nicotinamide adenine dinucleotide-cytochrome b_5 reductases. *Biochemistry 13*, 1701−1710.
(32) Iyanagi, T., and Mason, H. S. (1973) Some properties of hepatic reduced nicotinamide adenine dinucleotide phosphate-cytochrome *c* reductase. *Biochemistry 12*, 2297−2308.
(33) Yasukochi, Y., Peterson, J. A., and Masters, B. S. (1979) NADPH-cytochrome *c* (P-450) reductase. Spectrophotometric and stopped flow kinetic studies on the formation of reduced flavoprotein intermediates. *J. Biol. Chem. 254*, 7097−7104.
(34) Vermilion, J. L., Ballou, D. P., Massey, V., and Coon, M. J. (1981) Separate roles for FMN and FAD in catalysis by liver microsomal NADPH-cytochrome P-450 reductase. *J. Biol. Chem. 256*, 266−277.
(35) Oprian, D. D., and Coon, M. J. (1982) Oxidation-reduction states of FMN and FAD in NADPH-cytochrome P-450 reductase during reduction by NADPH. *J. Biol. Chem. 257*, 8935−8944.
(36) Bhattacharyya, A. K., Lipka, J. J., Waskell, L., and Tollin, G. (1991) Laser flash photolysis studies of the reduction kinetics of NADPH:cytochrome P-450 reductase. *Biochemistry 30*, 759−765.
(37) Gutierrez, A., Lian, L. Y., Wolf, C. R., Scrutton, N. S., and Roberts, G. C. (2001) Stopped-flow kinetic studies of flavin reduction in human cytochrome P450 reductase and its component domains. *Biochemistry 40*, 1964−1975.
(38) Gutierrez, A., Paine, M., Wolf, C. R., Scrutton, N. S., and Roberts, G. C. (2002) Relaxation kinetics of cytochrome P450 reductase: internal electron transfer is limited by conformational change and regulated by coenzyme binding. *Biochemistry 41*, 4626−4637.
(39) Gutierrez, A., Grunau, A., Paine, M., Munro, A. W., Wolf, C. R., Roberts, G. C., and Scrutton, N. S. (2003) Electron transfer in human cytochrome P450 reductase. *Biochem. Soc. Trans. 31*, 497−501.
(40) Bilimoria, M. H., and Kamin, H. (1973) The effect of high salt concentrations upon cytochrome *c*, cytochrome b_5, and iron-EDTA reductase activities of liver microsomal NADPH-cytochrome *c* reductase. *Ann. N.Y. Acad. Sci. 212*, 428−448.
(41) Black, S. D., French, J. S., Williams, C. H., Jr., and Coon, M. J. (1979) Role of a hydrophobic polypeptide in the N-terminal region of NADPH-cytochrome P-450 reductase in complex formation with P-450LM. *Biochem. Biophys. Res. Commun. 91*, 1528−1535.
(42) Black, S. D., and Coon, M. J. (1982) Structural features of liver microsomal NADPH-cytochrome P-450 reductase. Hydrophobic domain, hydrophilic domain, and connecting region. *J. Biol. Chem. 257*, 5929−5938.
(43) Korzekwa, K. R., Krishnamachary, N., Shou, M., Ogai, A., Parise, R. A., Rettie, A. E., Gonzalez, F. J., and Tracy, T. S. (1998) Evaluation of atypical cytochrome P450 kinetics with two-substrate models: evidence that multiple substrates can simultaneously bind to cytochrome P450 active sites. *Biochemistry 37*, 4137−4147.
(44) Roberts, A. G., Yang, J., Halpert, J. R., Nelson, S. D., Thummel, K. T., and Atkins, W. M. (2011) The structural basis for homotropic and heterotropic cooperativity of midazolam metabolism by human cytochrome P450 3A4. *Biochemistry 50*, 10804−10818.

DOI: 10.1021/acs.biochem.5b00510
Biochemistry 2015, 54, 4083−4096

(45) Davydov, D. R., Rumfeld, J. A. O., Sineva, E. V., Fernando, H., Davydova, N. Y., and Halpert, J. R. (2012) Peripheral ligand binding site in cytochrome P450 3A4 located with fluorescence resonance energy transfer (FRET). *J. Biol. Chem. 287*, 6797−6809.
(46) Denisov, I. G., Grinkova, Y. V., Baylon, J. L., Tajkhorshid, E., and Sligar, S. G. (2015) Mechanism of drug−drug interactions mediated by human cytochrome P450 CYP3A4 monomer. *Biochemistry 54*, 2227−2239.
(47) Black, S. D., Martin, S. T., and Smith, C. A. (1994) Membrane topology of liver microsomal cytochrome P450 2B4 determined via monoclonal antibodies directed to the halt-transfer signal. *Biochemistry 33*, 6945−6951.
(48) Shank-Retzlaff, M. L., Raner, G. M., Coon, M. J., and Sligar, S. G. (1998) Membrane topology of cytochrome P450 2B4 in Langmuir-Blodgett monolayers. *Arch. Biochem. Biophys. 359*, 82−88.
(49) Headlam, M. J., Wilce, M. C., and Tuckey, R. C. (2003) The F-G loop region of cytochrome P450scc (CYP11A1) interacts with the phospholipid membrane. *Biochim. Biophys. Acta 1617*, 96−108.
(50) Berka, K., Hendrychova, T., Anzenbacher, P., and Otyepka, M. (2011) Membrane position of ibuprofen agrees with suggested access path entrance to cytochrome P450 2C9 active site. *J. Phys. Chem. A 115*, 11248−11255.
(51) Cojocaru, V., Balali-Mood, K., Sansom, M. S., and Wade, R. C. (2011) Structure and dynamics of the membrane-bound cytochrome P450 2C9. *PLoS Comput. Biol. 7*, e1002152.
(52) Berka, K., Paloncyova, M., Anzenbacher, P., and Otyepka, M. (2013) Behavior of human cytochromes P450 on lipid membranes. *J. Phys. Chem. B 117*, 11556−11564.
(53) Monk, B. C., Tomasiak, T. M., Keniya, M. V., Huschmann, F. U., Tyndall, J. D., O'Connell, J. D., III, Cannon, R. D., McDonald, J. G., Rodriguez, A., Finer-Moore, J. S., and Stroud, R. M. (2014) Architecture of a single membrane spanning cytochrome P450 suggests constraints that orient the catalytic domain relative to a bilayer. *Proc. Natl. Acad. Sci. U.S.A. 111*, 3865−3870.
(54) Davydov, D. R., Davydova, N. Y., Sineva, E. V., and Halpert, J. R. (2015) Interactions among cytochromes P450 in microsomal membranes: Oligomerization of cytochromes P450 3A4, 3A5 and 2E1 and its functional consequences. *J. Biol. Chem. 290*, 3850−3864.
(55) Davydov, D. R., Davydova, N. Y., Sineva, E. V., Kufareva, I., and Halpert, J. R. (2013) Pivotal role of P450−P450 interactions in CYP3A4 allostery: the case of alpha-naphthoflavone. *Biochem. J. 453*, 219−230.
(56) Voznesensky, A. I., and Schenkman, J. B. (1992) Inhibition of cytochrome-P450 reductase by polyols has an electrostatic nature. *Eur. J. Biochem. 210*, 741−746.
(57) Voznesensky, A. I., and Schenkman, J. B. (1992) The cytochrome P450 2B4-NADPH cytochrome P450 reductase electron transfer complex is not formed by charge-pairing. *J. Biol. Chem. 267*, 14669−14676.
(58) Voznesensky, A. I., and Schenkman, J. B. (1994) Quantitative analyses of electrostatic interactions between NADPH-cytochrome P450 reductase and cytochrome P450 enzymes. *J. Biol. Chem. 269*, 15724−15731.
(59) Voznesensky, A. I., Schenkman, J. B., Pernecky, S. J., and Coon, M. J. (1994) The NH_2-terminal region of rabbit CYP2E1 is not essential for interaction with NADPH-cytochrome P450 reductase. *Biochem. Biophys. Res. Commun. 203*, 156−161.
(60) Eberhart, D. C., and Parkinson, A. (1991) Cytochrome P450 IIIA1 (P450p) requires cytochrome b_5 and phospholipid with unsaturated fatty acids. *Arch. Biochem. Biophys. 291*, 231−240.
(61) Maenpaa, J., Hall, S. D., Ring, B. J., Strom, S. C., and Wrighton, S. A. (1998) Human cytochrome P450 3A (CYP3A) mediated midazolam metabolism: the effect of assay conditions and regioselective stimulation by alpha-naphthoflavone, terfenadine and testosterone. *Pharmacogenetics 8*, 137−155.

DOI: 10.1021/acs.biochem.5b00510
Biochemistry 2015, 54, 4083−4096